Eur. Phys. J. D **3**, 257–265 (1998)

THE EUROPEAN PHYSICAL JOURNAL D

Photofragmentation of hydrated iron ions $Fe(H_2O)_n^+$ ($n = 1-9$) at 532, 355 and 266 nm

L. Dukan, L. del Fabbro, P. Pradel, O. Sublemontier, J.M. Mestdagh[a], and J.P. Visticot

CEA, DSM/DRECAM/SPAM, Bâtiment 522, CE Saclay, 91191 Gif-sur-Yvette Cedex, France

Received: 11 November 1997 / Revised: 18 February 1998 / Accepted: 22 April 1998

Abstract. Photofragmentation of $Fe(H_2O)_n^+$ clusters ($n = 1-9$) is investigated at three different wavelengths, 532, 355 and 266 nm. Two fragmentation pathways are observed depending essentially on the photon energy, but also on the parent size n. The fragmentation products belong to two ion families, $Fe(H_2O)_m^+$ and $FeOH(H_2O)_m^+$, which correspond to dehydration and intracluster dehydrogenation reactions respectively. The ion yields are studied as a function of the laser fluence in order to determine the number of photons implied in the photofragmentation process. This allows us to estimate that the $D[(H_2O)_{n-1}Fe^+-(H_2O)]$ bond energy is ranging between 0.44 eV and 0.55 eV for $5 \leq n \leq 9$. Photon absorption cross sections are also derived from the fluence experiments, and two different behaviors are observed: i) At 355 nm, far away from any Fe^+ transition, progressive solvation of the metal ion results in an increasing absorption cross section from $n = 2$ to $n = 9$. This can be attributed to a forbidden transition of bare Fe^+, which becomes progressively allowed because of the interaction with more and more water ligands. ii) At 266 nm, close to several allowed transitions of bare Fe^+, a distinct maximum is observed for the absorption of $Fe(H_2O)_2^+$ ion. It may be attributed to a change in the spin multiplicity when switching from Fe^+ and $Fe(H_2O)^+$ on one hand to $Fe(H_2O)_{n\geq 2}^+$ on the other.

PACS. 36.40.-c Atomic and molecular clusters – 82.30.-b Specific chemical reactions; reaction mechanisms

1 Introduction

Solvation of metal cation by water molecules has attracted the attention over the last ten years, both in experimental [1–8] and theoretical [9–17] works. Thermodynamic and structural properties of $M^+(L)_n$ species where M is the metal and L a ligand (water in particular), are reviewed in reference [18]. Most thermodynamical data were deduced from threshold energy measurements in a guided ion beam apparatus. This concerns alkali ions essentially [1,6,8], but also cations of transition metals [4, 5]. Bond energies $M^+(H_2O)_{n-1}-(H_2O)$ have been determined for M = Li, Na, K, Rb, Cs, Mg, Al, Ti-Cu and $n \leq 4$ (or 6).

Solvation of metal cations has also been studied by the photofragmentation technique, where water molecules are photodetached from $M^+(H_2O)_n$ clusters by visible light [19–24]. Spectroscopic, structural and chemical properties of monohydrated alkali and alkaline earth ions have been investigated by this technique, the cluster ions Mg^+-H_2O [20] and Ca^+-H_2O for instance [19]. More solvated species such as $Mg^+(H_2O)_n$ ($n = 1-5$) [22] and $Ca^+(H_2O)_n$ ($n = 1-6$) [23] have been investigated also. Large spectral shifts and band splitting are observed when switching from monosolvated to polysolvated alkali and alkaline earth ions. Other solvated metal ions, such as $V(H_2O)^+$ have been studied by Brucat *et al.* [25]. A different behavior is observed, where the solvation seems to allow transitions, which are normally forbidden for the bare metal ions. Similar behavior is reported for other metal ions [26,27].

Evaporation of water molecules is not the unique process to occur upon laser irradiation of $M(H_2O)_n^+$ cluster ions. Dehydrogenation is also observed where $MOH(H_2O)_m^+$ is the product [22,23].

The present study aims to investigate both these processes for hydrated iron ions $Fe(H_2O)_n^+$ ($n = 1-9$) generated in a laser evaporation source. Experimental and theoretical data are already available for these species, for n ranging between 1 and 4 [4,5,14], and provide information on geometry, binding energies of the water ligands and electronic structures. The present work allows investigation of clusters for a larger number of ligands, up to 9 water molecules. The cluster ions are photofragmented at 3 wavelengths, 532, 355 and 266 nm, and the relative yields of the dehydrogenation and dehydration reactions as well as the photofragment distribution are documented. The fluence of the photofragmentation laser was varied systematically in order to establish whether the photofragmentation processes are single or multi-photon processes.

[a] e-mail: jmm@santamaria.saclay.cea.fr

Absolute cross sections of the single photon processes are determined, and finally, an estimate is given of the binding energy of water molecules to the Fe^+ ions.

2 Experiment

The experimental setup has been described elsewhere [28]. Shortly, the cluster ions are produced in a laser vaporization source, where the doubled output of a pulsed Nd:YAG laser is focused on a rotating iron rod. The laser operates at a repetition rate of 10 Hz. The plasma formed by the laser impact is extracted by a mixture of helium and water coming from a pulsed valve. A supersonic expansion of the gas mixture proceeds through a 2 mm nozzle. This source generates the various families of clusters reported in reference [29]. The $Fe(H_2O)_n^+$ ions have the largest intensities. Weaker peaks are observed for the $FeOH(H_2O)_n^+$, $FeH(H_2O)_n^+$, $Fe_2(H_2O)_n^+$ and $Fe_3(H_2O)_n^+$ ions.

The beam carrying the cluster ions is collimated by two skimmers before entering into the extraction zone where positive ions are deflected into a reflectron TOF mass spectrometer. The mass spectrometer has a focusing zone located in the field free region between the extraction zone and the reflection zone. It allows us to irradiate the ions using the photofragmentation laser. Deflection plates are set 12 cm before the photofragmentation zone. At this location, the ion packets corresponding to the various families of cluster ions present in the beam are well separated from each other. A pulsed voltage is applied on the deflection plates. Its time width allows us to preselect ions of mass $Fe(H_2O)_n^+ \pm 2$ a.m.u., for any value of n ranging between 1 and 9. The field free region between the extraction zone and the deflection plates plays indeed the role of a linear TOF-MS prior laser irradiation.

The desired ions $Fe(H_2O)_n^+$ are irradiated *specifically among the preselected ions* with the photofragmentation laser (Nd:YAG, Quantel 581C-10) when the timings between the ion extraction, the deflection plates and the photofragmentation laser are set correctly. The timing of the deflection plates preselects the mass range $Fe(H_2O)_n^+$ ± 2 a.m.u. as said above, and the exact timing of the photofragmentation laser allows us to illuminate the interaction zone only when the ion packet corresponding to the desired parent ions $Fe(H_2O)_n^+$ is filling exactly the interaction zone. The dimensions of the laser beam are such that the height and width of the laser pulse matches exactly the dimensions of the $Fe(H_2O)_n^+$ ion packet. For this purpose, the laser beam is collimated by a rectangular aperture (5×10 mm^2) corresponding to $Fe(H_2O)_n^+$. Furthermore, special attention is given, so the aperture illumination is uniform. This is checked by using a camera, on which the aperture was imaged. Experiments performed with and without the aperture demonstrate that all the $Fe(H_2O)_n^+$ ions present in the ion packet experience the photon flux. These precautions are necessary to extract absolute cross sections from the fluence experiments reported below.

All the ions, parent and products are detected after the reflectron. In order to detect the parent and the product ions with the same resolution, and also to unambiguously determine the product masses, the following procedure is used. The voltage applied to the reflectron is adjusted for the detection of each product ion, so the product of mass m_d with the adjusted voltage V_d has the same trajectory in the reflectron, *i.e.* the same time of flight than the parent ions of mass m_p with the original voltage V_p. The relationship between V_d, V_p, m_d and m_p is given by

$$V_d = V_p \frac{m_d}{m_p} \cdot \tag{1}$$

The ratio of the peak integrals measured with the potential V_d and V_p represents the fragmentation ratio into the product ion of mass m_d.

A beam attenuator is placed on the laser beam to vary the laser fluence, and a calibrated calorimeter allows us to measure the absolute fluence of the laser beam passing through the rectangular aperture.

The photofragmentation laser is operated at half the frequency of the ablation laser (*i.e.* 5 Hz). As a results, photofragmentation is turn on every two shots of the ablation laser. The ion signal (parent or product ions) is collected by a two channel 200 MHz digitizer (Sony-Tektronix RTD 710). The first channel records the parent ion signal with the photofragmentation laser turned off and the reflectron voltage tuned to V_p. The second channel records the ion signal with the photofragmentation laser turned on and the reflectron voltage tuned either to V_p for measuring the parent attenuation or to V_d for measuring the product ion signal. Signals are averaged over 1024 shots of the ablation laser. Channel 1 is used to calibrate the signal recorded in channel 2, the desired signal corresponding to the ratio I_2/I_1 of the integrals of the peaks recorded in channels 1 and 2.

Two types of experiments are performed:

- In the first one, the fluence of the photofragmentation laser is set to its maximum. At this fluence, both single and multi-photon processes are present. The attenuation of the parent ion is given by the ratio between channel 2 and channel 1 when tuning the reflectron voltage to V_p all the time. The relative integrals of the various product ions are obtained by switching the reflectron voltage to V_d when recording channel 2. The experiment is reproduced for each product ion by using the proper value of V_d. The purpose of this series of experiment is to observe the nature of the fragments that are produced when illuminating the $Fe(H_2O)_n^+$ ions, whatever the number of photons involved in the photofragmentation process.
- The second experiment consists in measuring ion signals (parent or product ions) as a function of the fluence of photofragmentation laser. We first record the heavier fragment signal with the maximum of fluence. Then this signal is recorded for decreasing values of the fluence until the signal vanishes. Again, the same experiment is repeated for each fragment by setting V_d to the proper value. The purpose of this series of

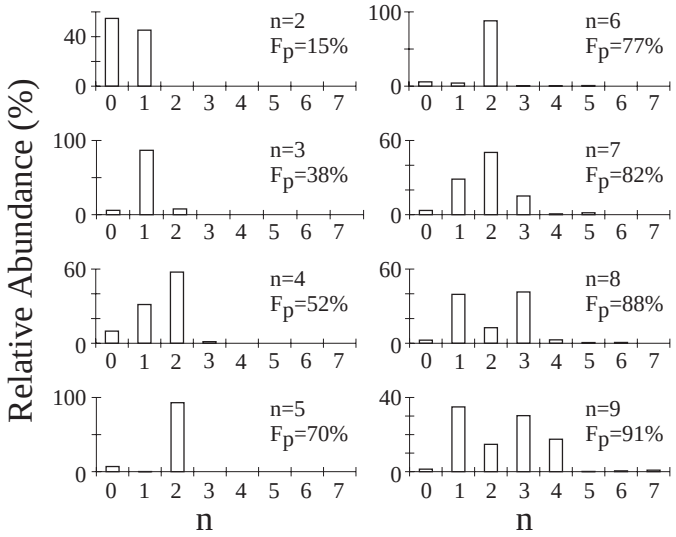

Fig. 1. Relative abundance of the product ions in the fragmentation of the parent ions $Fe(H_2O)_n^+$ at 355 nm. Each panel corresponds to a different parent ion, as labeled in the figure, The x axis gives the number of water molecule m of the product ions $Fe(H_2O)_m^+$. The quantity F_p indicated in each panel is the fraction of the parent $Fe(H_2O)_n^+$ that is photofragmented at this wavelength. The laser fluence is maximum, and the observed intensities reflect both single and multi-photon processes.

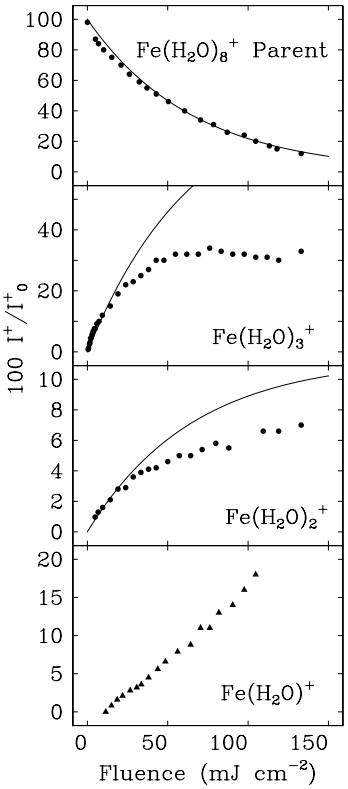

Fig. 2. Photofragmentation of the $Fe(H_2O)_8^+$ cluster ion at 355 nm. The top panel shows the decay of the parent ion as a function of the laser fluence. The solid curve going through the data points is the best fit obtained using expression 2. The other panels show the variation of the product ion signal as labeled in each panel. The solid line in panels $Fe(H_2O)_3^+$ and $Fe(H_2O)_2^+$ best fits the the experimental points using expression (3) and considering the laser fluences smaller than 20 mJ cm^{-2} where population of these ions by a single photon process is expected.

experiments is to distinguish between single and multi-photon processes. Ultimately, absolute photofragmentation cross sections are determined for the single photon processes.

3 Results

3.1 Photofragmentation at 532 nm

The photon energy at 532 nm is 2.33 eV, and the fluence of the unattenuated laser at this wavelength is 350 mJ/cm^2. Almost no photofragmentation of the parent clusters $Fe(H_2O)_n^+$ is observed. Only the largest parent ion, $Fe(H_2O)_9^+$ is attenuated by less than 10%. Such fragmentation yield is too small to deserved a systematic study as a function of the laser fluence.

3.2 Photofragmentation at 355 nm

The photon energy at 355 nm is 3.49 eV, and the fluence of the unattenuated laser at this wavelength is 130 mJ/cm^2.

The laser irradiation actually photofragments the parent clusters $Fe(H_2O)_n^+$, which are attenuated by a factor F_p when the laser fluence is maximum. The resulting series of product ions are shown in Figure 1, together with the factor F_p. The figure reflects both single and multi-photon processes. Several points must be done from the figure. The heavier parents are more strongly attenuated than the small one: only 15% of the $Fe(H_2O)_2^+$ ions are fragmented whereas more than 90% of the $Fe(H_2O)_9^+$ ions do so. Whatever the number n of water molecules in the parent ion, the product ions correspond to the series $Fe(H_2O)_m^+$ with $m < n$. Evaporation of water molecules is thus the dominant photofragmentation process at this wavelength. The dehydrogenation process leading to the $FeOH(H_2O)_m^+$ series is also observed. The branching ratio to this channel is significant and reach 8% only for $Fe(H_2O)_{3,4}^+$ parents. It is as low as 2% for $Fe(H_2O)_{8,9}^+$, and not measurable for the other parent sizes. Such small branching ratios are too small to be studied quantitatively in a fluence experiment.

The decay of the $Fe(H_2O)_{2-9}^+$ parent ions has been studied as a function of the laser fluence, as well as the increase of the product ion signal when intense enough to be studied in such an experiment. An example is shown in Figure 2 for the parent $Fe(H_2O)_8^+$ and its product ions $Fe(H_2O)_3^+$, $Fe(H_2O)_2^+$ and $Fe(H_2O)^+$. An exponential decrease of the parent ion is observed, as well as an increase of the fragment populations.

Table 1. Total photofragmentation cross sections σ at 355 nm and partial cross sections σ_d in units of 10^{-18} cm^2. Processes requiring more than one photon are indicated by > 1. No cross section is indicated for fragments that are associated with a too small intensity.

Parents $Fe(H_2O)_n^+$	Parents σ	Fragments $Fe(H_2O)_m^+$ σ_d			
		1	2	3	4
2	0.55				
3	2.1	1.9			
4	3.2	0.83	1.4		
5	4.7		3.8		
6	6.2		4.6		
7	7.7	> 1	4.0	2.2	
8	8.5	> 1	1.0	7.3	
9	8.8	> 1	> 1	5.4	2.5

The exponential decay of the parent ion is representative of a single photon process. The photofragmentation cross section of the parent ions by a single 355 nm photon can thus be extracted according to the following expression:

$$\frac{I^+}{I_0^+} = \exp(-\frac{\sigma}{h\nu}\frac{W_L}{S}) \qquad (2)$$

where I_0^+ is the laser-off intensity of the parent peak and I^+ its laser-on intensity. W_L is the laser energy and S the cross section of the laser beam. Finally, $h\nu$ is the photon energy and σ is the desired photofragmentation cross section. The quality of the fit obtained using this expression appears in Figure 2. It indicates that the photofragmention of the parent is monophotonic over the full range of fluences explored experimentally. Furthermore the nice fit obtained, and the fact that up to 90% of the parent could be attenuated suggest that a unique class of ions is interacting with the laser. A forthcoming series of experiments performed on the photofragmentation of $Co(H_2O)_n^+$ ions will illustrate a different behavior.

The cross sections σ that best fits experimental data similar to those reported in Figure 2 are shown both in Table 1 and Figure 3. A general increase of the cross sections with the number of ligands n is observed, with values ranging between 0.55 and 8.8×10^{-18} cm^2.

Product ion signals produced by a single photon process must be adequately described by the expression:

$$\frac{I_d^+}{I_0^+} = \frac{\sigma_d}{\sigma}\left[1 - \exp(-\frac{\sigma}{h\nu}\frac{W_L}{S})\right] \qquad (3)$$

where σ_d is the partial cross section for forming the product ions under consideration. Such expression well account for the observation of Figure 2 for the $Fe(H_2O)_2^+$ and $Fe(H_2O)_3^+$ product ions, at low fluence when the single photon process is dominant. The deviation observed in the figure for laser fluences larger than 20 mJ/cm^2 is simply interpreted as the absorption of a second photon by the fragment. Multiphoton photofragmentations thus appear as sequential absorptions where a first photon is absorbed by the parent ions $Fe(H_2O)_8^+$ in Figure 2 and initiates the fragmentation, thus forming primary photofragmentation products $Fe(H_2O)_2^+$ and $Fe(H_2O)_3^+$ in Figure 2. A second photon is absorbed by the primary products when the laser fluence is large enough, thus forming secondary photofragmentation products $Fe(H_2O)^+$ in Figure 2. The secondary photon absorption results into a depletion of the primary product population as observed in the figures when comparing the population measured experimentally to that expected from only a single photon process. A further point must be done. Of course, secondary products are never accounted by the single photon expression (3). This is actually observed in Figure 2 when considering the fragment $Fe(H_2O)^+$.

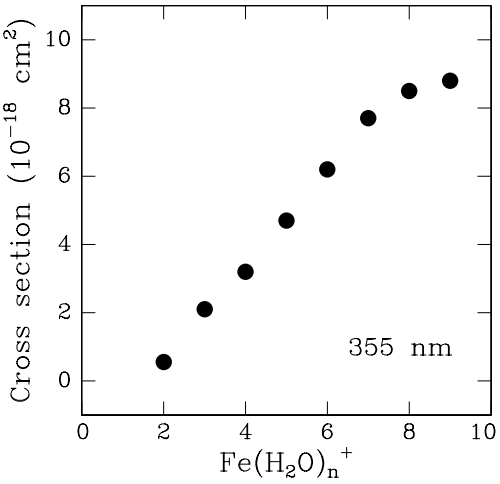

Fig. 3. Photofragmentation cross section of the parent ions $Fe(H_2O)_n^+$ as a function of n when the laser wavelength is 355 nm.

The partial cross sections σ_d that best fit experimental data similar to those of Figure 2 are listed in Table 1. As above, the fit is performed at fluences smaller than 20 mJ/cm^2, when expression (3) adequately fits the experimental data, *i.e.* when the product is populated by a single photon from the parent ion. It appears in the table that the sum of the product cross sections is systematically smaller than the total photofragmentation cross sections of the parent ion. This is due to losses of product ions both in the irradiation zone and in the reflectron. The photofragmentation process is indeed likely to communicate excess kinetic energy to these ions, which results into losses. Of course this affect the accuracy of the cross section measurements by making the measured product cross sections systematically smaller than the real one. Uncertainties of 30% have been estimated to account for this effect.

3.3 Photofragmentation at 266 nm

The 355 nm experiments have also been conducted at 266 nm. The photon energy is then 4.66 eV and the maximum laser fluence is 70 mJ/cm^2.

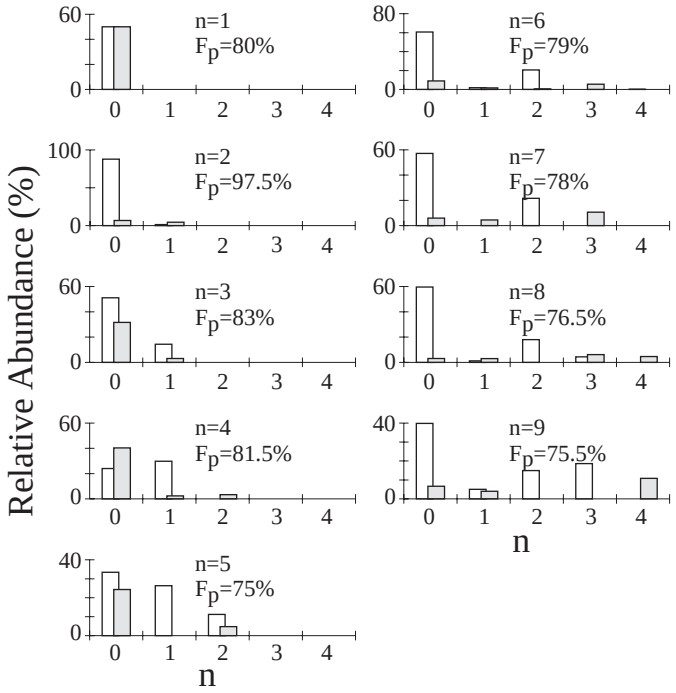

Fig. 4. Same caption as Figure 1 for the photofragmentation at 266 nm. The product ions in white corresponds to the series $Fe(H_2O)_m^+$ (dehydration process) and those is grey to $FeOH(H_2O)_m^+$ (dehydrogenation reactions).

The photofragmentation yield F_p, and the relative populations of the photofragmentation products observed at this wavelength are shown in Figure 4. This experiment was performed with the maximum laser fluence, the parents observed and their relative populations are the consequence both of single and multi-photon processes. These results at 266 nm contrast with the corresponding one shown above at 355 nm. Very large values of F_p ranging between 80 and 97.5 % are observed at 266 nm: $Fe(H_2O)_2^+$ is associated with the largest photofragmentation efficiency, and a slow decrease follows from $Fe(H_2O)_3^+$ to $Fe(H_2O)_9^+$. Moreover, two classes of fragments are identified, which correspond to evaporation of water molecules (white bars in the figure) and to an intracluster dehydrogenation reaction (grey bars). The corresponding formula are $Fe(H_2O)_m^+$ and $FeOH(H_2O)_m^+$ respectively. The dehydration pathway generally, but not systematically, dominates the dehydrogenation reaction.

Let us consider the dehydration products first (white bars of Fig. 4). As before at 355 nm, the number of water molecules lost by the parent ions increases with the initial size of the ion. However, the size of the dehydration products are systematically smaller at 266 nm than at 355 nm. In particular, bare Fe^+ is almost always the most abundant dehydration product at 266 nm whereas it is one of less abundant fragment at 355 nm.

Dehydrogenation products $FeOH(H_2O)_m^+$ are detected for all the parent ions $Fe(H_2O)_{n=1,\ldots,9}^+$ (Fig. 4). This pathway is particularly intense when $n \leq 5$, reaching a relative intensity of 50% for $FeOH^+$ in the photofragmentation of the $Fe(H_2O)^+$ parent ion. For most parents, dehydrogenation products are the heaviest fragments detected.

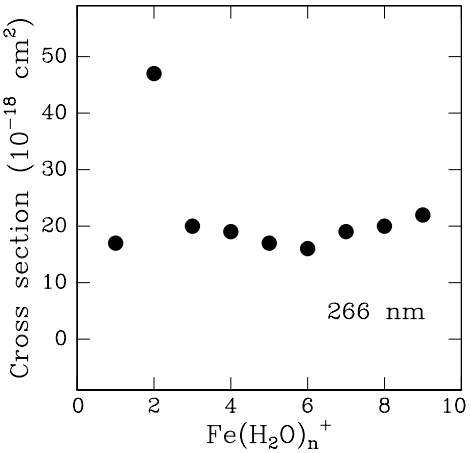

Fig. 5. Same caption as Figure 3 for the photofragmentation at 266 nm.

A fluence experiment has been conducted at 266 nm. As before in the 355 nm experiment, photofragmentation cross sections are deduced from the fluence experiment for the single photon processes. The corresponding results are shown in Figure 5 for the parent ions $Fe(H_2O)_n^+$ ($1 \leq n \leq 9$). The substantially larger cross section measured for $n = 2$ is not an artifact of the experiment. Its origin is discussed in Section 4.3.1. These cross sections are also shown in the second column of Table 2, together with partial cross sections of product formation. From Table 2 we know that most of the single photon processes lead to dehydration products bearing one to three water ligands. Interestingly, the formation of bare Fe^+ ions is always a multi-photon process for parent clusters larger than $Fe(H_2O)_3^+$. Table 2 also shows that the dehydrogenation reactions are multi-photon processes, except in two cases: single-photon reactions prevail for the loss of one H-atom by $Fe(H_2O)^+$ and $Fe(H_2O)_2^+$. Partial cross sections for forming these fragments are also shown in Table 2.

As in Table 1, and for the same reason, the sum of the partial cross sections is, but in one case, always smaller than the photofragmentation cross section of the parent ions. This sets an upper limit of 30% to the accuracy of the cross sections listed in Table 2.

4 Discussion

4.1 Photofragmentation pathways

The results obtained in the previous section show that the $Fe(H_2O)_n^+$ parent ions decay into two families of product ions, when absorbing 355 or 266 nm photons. The first family, which is dominant at 266 nm and almost exclusive at 355 nm, corresponds to a dehydration reaction:

$$Fe(H_2O)_n^+ + h\nu \rightarrow Fe(H_2O)_m^+ + (n-m)H_2O. \quad (4)$$

Table 2. Same caption as Table 1 for the photofragmentation at 266 nm.

Parents $Fe(H_2O)_n^+$	Parents σ	Fragments $Fe(H_2O)_m^+$ σ_d				Fragments $FeOH(H_2O)_m^+$ σ_d				
		0	1	2	3	0	1	2	3	4
1	17	6.3				15				
2	46.3	33	1.0			> 1	2.8			
3	20	7.0	9.4			> 1				
4	19	> 1	12.5			> 1				
5	17.2	> 1	7.4	5.4		> 1		> 1		
6	15.7	> 1		11.7		> 1				
7	18.7	> 1		12.0		> 1	> 1		> 1	
8	19.6	> 1		10.1	2.9	> 1	> 1			> 1
9	21.6	> 1		6.3	8.0					> 1

The second family is significant at 266 nm only and corresponds to the intracluster dehydrogenation reaction

$$Fe(H_2O)_n^+ + h\nu \rightarrow FeOH(H_2O)_m^+ + H + (n-m-1)H_2O. \quad (5)$$

The two photofragmentation channels above have already been reported for other hydrated metal species such as $Ca(H_2O)_n^+$ and $Mg(H_2O)_n^+$ [22,23]. The evaporation process is dominant for $Ca(H_2O)_n^+$ whereas the dehydrogenation reaction is the major pathway for $Mg(H_2O)_n^+$ complexes.

The dehydration and the dehydrogenation processes observed in the present work result either from single photon or from multi-photon absorption. We focus the discussion on the single photon absorption exclusively, and therefore, we concentrate on those product ions listed in Tables 1 and 2 where partial cross sections are given.

The existing literature allows to built the energy diagram shown in Figure 6 for the photofragmentation of the $Fe(H_2O)^+$ ions. Four products are energetically accessible for single 266 nm photon absorption: Fe^+, $FeOH^+$, FeO^+ and FeH^+ among which, only $FeOH^+$ and Fe^+ are observed experimentally.

The largest cross section corresponds to the $FeOH^+$ formation, which is not to the most exoergic fragmentation pathway of $Fe(H_2O)^+$. This suggests that the photon energy is not redistributed statistically among the accessible phase space otherwise indeed, formation of Fe^+ would have been favored over that of $FeOH^+$. Photofragmentation of larger parent clusters behave differently, since the dehydrogenation channel is not favored over the dehydration for $Fe(H_2O)_2^+$, and is no longer accessed in a single 266 nm photon absorption for $Fe(H_2O)_{n\geq 3}^+$.

Finally, FeH^+ is not observed experimentally, in spite of 0.3 eV exoergicity when 266 nm photon are absorbed by the $Fe(H_2O)^+$ ion. A possible interpretation is that the excited potential surface that is reached with this excitation does not correlate to the FeH^+ formation in the exit channel of the reaction.

Reaction of $Fe^+(a^6D, a^4F)$ with D_2O forming FeD^+ and $FeOD^+$ has been studied by Armentrout and coworker [30]. These authors have discussed qualitative

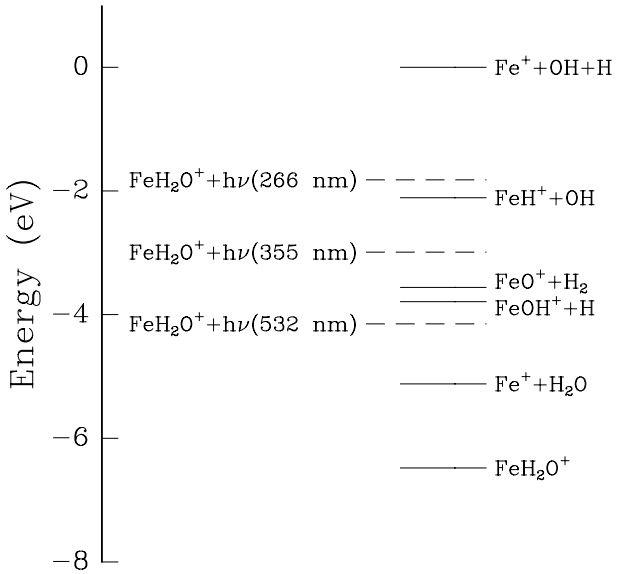

Fig. 6. Energetics of the $Fe(H_2O)^+$ dehydrogenation processes. The bond energies used to build the diagram are taken from the following references [5] (Fe^+-H_2O), [30] (Fe^+-OH and Fe^+-O), [33] (Fe^+-H), [34] (H−OH), [35] (H−H and O−H).

potential energy surfaces to account for their experimental results. The reaction path proceeds along a quartet potential surface. It first goes through exoergic formation of the $Fe(D_2O)^+$ adduct, then it overcomes an activation barrier of about 3 eV above the energy of the adduct, and reaches the inserted intermediate $D-Fe^+-OD$, which correlates to the products FeD^+ and $FeOD^+$ with no further barrier except the barrier of endoergicity. This mechanism cannot be used to interpret the results of the present work, since the potential surfaces involved here are entirely different. They correspond here to 3.49 eV and 4.66 eV electronic excitation (resp. for the 355 and 266 nm photon absorption) whereas reaction in the work of Armentrout proceeds from the ground electronic state of $Fe^+(a^6D)$ or from a level that has only 0.25 eV electronic excitation (a^4F). The results presented here give some indication on the topography of the excited surface that is accessed by the 266 nm photon absorption of $Fe(H_2O)^+$. It allows a

reaction path to $FeOH^+$ and Fe^+, but not to FeH^+ or FeO^+.

4.2 Binding energies of water ligands

We concentrate now on the photofragmentation processes that result from a single photon absorption, with the aim of giving limits to binding energies of water ligands. More precisely, we observe in Tables 1 and 2 that multi-photon processes always appear for the smallest masses, *i.e.* after having broken a number of bonds. A simple explanation is that dehydration or dehydrogenation processes associated with more and more water evaporation becomes multi-photonic when their endoergicity is larger than the energy of a single photon absorbed by the parent ion. As a result, the limit between single and multi-photon processes can be used to put limits to the endoergicity of the process under consideration.

We consider the evaporation of water molecules from $Fe(H_2O)_4^+$ in the 266 nm experiment. From our experiment we know that evaporation of three water molecules is possible in a single photon absorption whereas evaporation of 4 water molecules requires a multi-photon absorption. This would suggest that the binding energy of 3 of the 4 water molecules $Fe(H_2O)_4^+$ is smaller than the 4.66 eV of the 266 nm photon whereas the binding energy of the 4 water molecules is larger than 4.66 eV.

The existing literature allows us to draw the energy diagram of the $Fe(H_2O)_{n\leq 4}^+$ ions shown in Figure 7 [5,14]. The figure indicates that the single photon evaporation of 3 water ligands is actually expected. In contrast, the fact that evaporation of 4 water molecules is multi-photonic, is surprising if assuming that the evaporation of the 4 water molecules forms the ground state ^6D of Fe^+. This result can be understood if assuming that the evaporation process is spin conserving. In this case, the Fe^+ ion would be formed in the excited ^4F state which correlate to the ground state of the $Fe(H_2O)_{n\geq 2}^+$ ions. We know indeed from the group of Bauschlisher that the ground states of $Fe(H_2O)_{n\geq 2}^+$ ions are quartet states whereas that of $Fe(H_2O)^+$ and Fe^+ are sextuplet states [14]. Spin conserving evaporation thus will result into formation of electronically excited $Fe(H_2O)^+$ and Fe^+.

Finally, we use the data of Table 1 to have insight into the binding energy of water in large systems: $Fe(H_2O)_{n-1}^+-(H_2O)$ when $n \geq 5$. The limit between single and multi-photon evaporations in Table 1 indicates that the evaporation of 6 water molecules from $Fe(H_2O)_8^+$ and $Fe(H_2O)_9^+$ is exoergic for one photon absorption whereas evaporation of 7 water molecules is endoergic. Therefore, the binding energy of 6 (resp. 7) water molecules both to $Fe(H_2O)_8^+$ and $Fe(H_2O)_9^+$ is smaller (resp. larger) than the photon energy (3.49 eV). From the work of Dalleska et al, we know the binding energy of water molecules in the $Fe(H_2O)_{n\leq 4}^+$ ions. The energy consideration that has just been done allows us to document the binding energy of one water molecules to larger cluster ions: $Fe(H_2O)_{4\leq n-1\leq 8}^+$. We assume that this binding energy is constant for $4 \leq n-1 \leq 8$. We thus deduce that its value

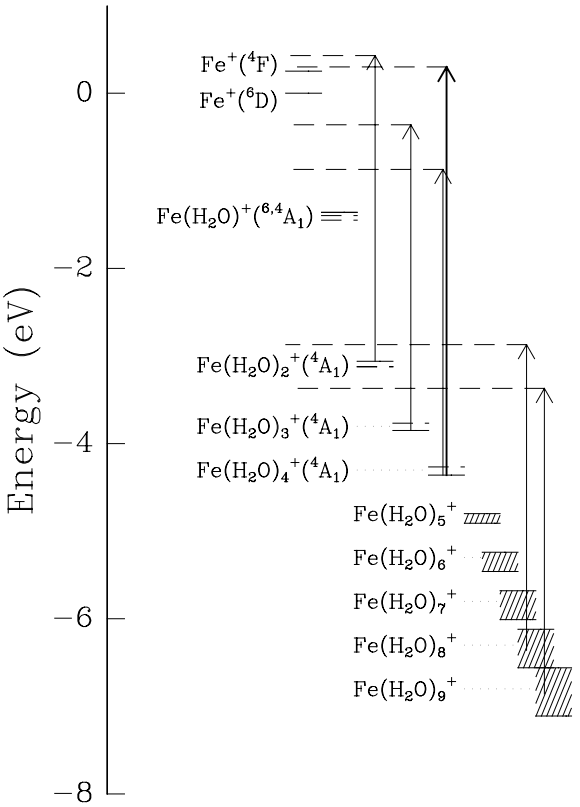

Fig. 7. Energetics of the dehydration of the $Fe(H_2O)_n^+$ cluster ions. The zero of energy corresponds to $Fe^+ + nH_2O$. The full (resp. dashed) horizontal lines are experimentally (resp. theoretically) determined energies. The data used for Fe^+ are taken from reference [36], those for $Fe(H_2O)_{1-4}^+$ from [5,14]. Finally those for $Fe(H_2O)_{5-9}^+$ are the upper and lower energy limits of the $Fe(H_2O)_{n-1}-H_2O$ bond determined in the present work. The bold arrow corresponds to the energy of 266 nm photons and the thin arrows to that of the 355 nm photons.

is in the range: 0.44-0.55 eV. The energetic location of the $Fe(H_2O)_{5\leq n\leq 9}^+$ ions is also reported in Figure 7 together with that of the $Fe(H_2O)_{n\leq 4}^+$ ions that we have already located using the existing literature [5,14]. The present estimate of the $Fe(H_2O)_{4\leq n-1\leq 8}^+-H_2O$ binding energies is in line with those found by previous investigations of $Fe(H_2O)_{n-1\leq 3}^+-H_2O$. The energies reported in the figure suggests a picture where water molecules surrounding Fe^+ beyond the fourth molecule, are forming a second solvation shell with no drastic change in the binding energy.

It is interesting to compare the binding energies of one water molecules in the second shell $Fe(H_2O)_n^+$ clusters estimated in the present work to the binding energy E_b per water molecule in neutral $(H_2O)_n$ clusters. Reference [31] shows that E_b (in eV) is well accounted by the expression

$$E_b = 0.49 - \frac{0.65}{n} \qquad (6)$$

and varies between 0.36 and 0.42 eV for n varying between 5 and 9. The range 0.44-0.55 eV estimated in the present work for the binding energy of one water molecule in $Fe(H_2O)_{n\geq 5}^+$ is only slightly larger than these values.

This strongly suggests that the cation charge is essentially screened by the four water molecules of the first solvation shell, making the water molecules of the outer shell very much H-bonded as in pure water clusters. Such convergence towards the H-bond energy of large pure water clusters has been encountered in many $X^+(H_2O)_n$ systems when the number of water molecules exceeds 4: $H_3O(H_2O)_n^+$ [32], $Li(H_2O)_n^+$ [8], Li, Na, K, $Rb(H_2O)_n^+$ [17] and $Al(H_2O)_n^+$ [6].

4.3 Effect of solvation on photon absorption

Section 4.2 has shown that most of the photon energy tends to be used to evaporate water molecules. Moreover, the binding energy of water molecules shown in Figure 7 and the calculation of references [12–14] does not suggest a strong electronic transfer from H_2O to Fe^+ even in the largest cluster ions. As a result, it seems appropriate to discuss the electronic structure of the $Fe(H_2O)_n^+$ ions in terms of the electronic structure of the bare Fe^+ cation, perturbed by water ligands. We use this picture as a guideline to discuss the absolute cross sections shown in Figures 3 and 5.

4.3.1 The 266 nm absorption

The cross section at this wavelength is ranging between 15 and 50×10^{-18} cm^2. Such large values indicate the occurrence of an allowed transition.

The resonance transition $a^6D \rightarrow z^6D$ of bare Fe^+ is located at 260 nm. Only a small red shift, or a broadening of the transition might account for the large absorption cross section measured to 266 nm. The increase of the cross section for $n = 2$ might indicate that the red shift for $n = 2$ moves the resonance almost exactly to 266 nm, whereas for $n = 1$ and $n \geq 3$ the resonance is not perfect. However, we shall see that this interpretation is oversimplified. Another one based on changes in spin multiplicities is discussed now.

Let us recall information about the electronic configuration of bare and hydrated Fe^+ ions. The ground state of the bare Fe^+ cation has the electronic configuration $a^6D(3d^64s^1)$. The $a^4F(3d^7)$ state is only 0.23 eV higher in energy. From theoretical calculations in the group of Bauschlicher, it appears that the sextuplet ground state is conserved for the monohydrated system $Fe(H_2O)^+$ which reduces the iron-ligand repulsion by means of $4s-4p$ polarization [12–14]. The presence of two and more H_2O ligands needs the $4s \rightarrow 3d$ promotion to overcome the metal ligand repulsion due to the interaction between H_2O orbitals and the iron $4s$ orbital. The $sd\sigma$ hybridisation leads to a quartet ground state for $Fe(H_2O)_{2\leq n\leq 4}^+$ ions.

When considering the spin state of the hydrated cation, the above interpretation based on a red shifted or a broadened resonance transition is probably valid to interpret the large photon absorption cross section of the monohydrated ion FeH_2O^+, since it has a sextuplet ground state as in bare Fe^+. In contrast, the large cross section measured with two and more ligated water molecules deserve another interpretation, since their ground states are quartet states. The population distributions calculated by Rosi and Bauschlicher [12–14] show that the ground state of the $Fe(H_2O)_2^+$ ion is a mixing of the electronic configurations $3d^64s$ and $3d^7$, which allow transitions from the states a^6D, a^4D ($3d^64s$) and $a^4F(3d^7)$. As a result, the resonance transition at 260 nm to the $z^6D(3d^64p)$ level still exists, but additional transitions appear between quartet states. In particular, transitions to $z^4F(3d^64p)$ and $z^4D(3d^64p)$ may be invoked. The a^4D-z^4F transition, at 271.6 nm in bare Fe^+ is certainly the dominant one.

The configuration mixing in more ligated species is certainly more complex than in the di-ligated one. This makes predictions hazardous about transitions for these ions. However, one point is clear from the experiment, the transition is still allowed at 266 nm for $Fe(H_2O)_{3\leq n\leq 9}$, but the oscillator strength decreases slightly as n increases.

4.3.2 The 355 nm absorption

The absorption cross section of the $Fe(H_2O)_n^+$ ions are much smaller in this series of experiments, and fall in the range $1-10 \times 10^{-18}$ cm^2. The general trend as n increases differ markedly also from what observed at 266 nm, since the cross sections increases steadily. A saturation seems to happen only for clusters carrying 7 to 9 water ligands.

The absorption cross section of the monohydrated ion is not reported in Figure 3 because it is too small to be measurable. As a result, the cross sections reported in Figure 3 all correspond to electronic transitions from a quartet ground state. The steady increase of the absorption cross section with n and the small value of the cross sections seem to be representative of a forbidden transition of the bare Fe^+ ion that becomes partially allowed when the number of water ligand increases. Such an interpretation where the presence of ligands allows a transition that is normally forbidden in the bare metal ion has already been proposed in the group of Brucat for the V^+ cation solvated by a single water molecule [25].

The enhancement of the oscillator strength by the ligand is due to a perturbation of the electronic levels of the metal ion by the water orbitals. Presence of ligands causes indeed a $d-p$ mixing leading to modification of the oscillator strengths. The iron ion has a forbidden transition around 340 nm between quartet states of the $(a^4F(3d^7) - b^4D(3d^64s))$. Of course, the interplay of $d-p$ mixing in one of these states would make the transition partially allowed.

4.3.3 The 532 nm absorption

Almost no photofragmentation is observed at this wavelength, although energetially allowed to do so. This indicates that in contrast to what observed at 355 nm, progressive solvation of Fe^+ by water molecules do not allows transitions, which are normally forbidden in the free ion.

5 Conclusion

An apparatus combining a laser evaporation source and a R-TOF mass spectrometer, has been used to observe the photofragmentation of hydrated metal ions $Fe(H_2O)_n^+$ at three wavelengths, 532, 355 and 266 nm.

No fragmentation is observed at 532 nm, and two photofragmentation channels are observed for the other two wavelengths: firstly, a simple water evaporation or dehydration reaction, which is the dominant process, and secondly, an intracluster dehydrogenation reaction which is only significant at 266 nm. The dehydrogenation process is always multi-photonic, except for $Fe(H_2O)^+$ and $Fe(H_2O)_2^+$ which fragments into $FeOH^+$ and $FeOH(H_2O)^+$ by absorption of a single 266 nm photon.

The fluence experiments are first used as a tool to determine whether the photofragmentation processes that are observed are mono- or multi-photonic. The threshold between single and multi-photon processes allows to give limits to the bond dissociation energy of water ligands to Fe^+: $D[(H_2O)_{n-1}Fe^+-(H_2O)]$, for $n \geq 5$, is ranging between 0.44 eV and 0.55 eV.

Energy considerations on the successive evaporation of water molecules from $Fe(H_2O)_n^+$ ions is consistent with the assumption that the evaporation process conserves the spin multiplicity of metal ion, which is a quartet when $n \geq 2$. As a result, evaporation of n water molecules would correlate to formation of bare Fe^+ ions, electronically excited in the $^4F(3d^7)$ state.

The other important point of the present study is the observation of two different effects when considering the photon absorption cross section of the $Fe(H_2O)_n^+$ clusters. An allowed transition is observed in the cluster ions at 266 nm, which results from the mixing of several electronic configurations of the bare ion. The larger cross section measured for the $Fe(H_2O)_2^+$ cluster has been attributed to a change of the spin multiplicity from sextuplet to quartet when the number of ligated water molecules is larger or equal to two. The effect of solvation on Fe^+ transitions at 355 nm is entirely different. It corresponds to a continuous enhancement of the cross section when the number of water ligands is increased. This behavior is attributed to a forbidden transition which becomes partly allowed because of state mixing when more and more water molecules are ligated to the iron ion.

References

1. I. Džidić, P. Kebarle, J. Phys. Chem. **74**, 1466 (1970).
2. P.J. Marinelli, R.R. Squires, J. Am. Chem. Soc. **111**, 4101 (1989).
3. T.F. Magnera, D.E. David, J. Michl, J. Am. Chem. Soc. **111**, 4100 (1989).
4. R.H. Schultz, P.B. Armentrout, J. Phys. Chem. **97**, 596 (1993).
5. N.F. Dalleska, K. Honma, L.S. Sunderlin, P.B. Armentrout, J. Am. Chem. Soc. **116**, 3519 (1994).
6. N.F. Dalleska, B.L. Tjelta, P.B. Armentrout, J. Phys. Chem. **98**, 4191 (1994).
7. A.S. Harms, S.N. Khanna, B. Chen, A.W. Castleman Jr, J. Chem. Phys. **100**, 3540 (1994).
8. M.T. Rodgers, P.B. Armentrout, J. Phys. Chem. **101**, 1238 (1997).
9. D. Feller, E.D. Glendening, R.A. Kendall, K.A. Peterson, J. Chem. Phys. **100**, 4981 (1994).
10. S.R. Bauschlicher Jr., C.W. Langhoff, H. Partridge, J. Chem. Phys. **94**, 2068 (1991).
11. C.W. Bauschlicher Jr., M. Sodupe, H. Partridge, J. Chem. Phys. **96**, 4453 (1992).
12. M. Rosi, C.W. Bauschlicher Jr., J. Chem. Phys. **90**, 7264 (1990).
13. M. Rosi, C.W. Bauschlicher Jr., J. Chem. Phys. **92**, 1876 (1990).
14. A. Ricca, C.W. Bauschlicher Jr., J. Phys. Chem. **99**, 9003 (1995).
15. E. Kochanski, E. Constantin, J. Chem. Phys. **87**, 1661 (1987).
16. H. Watanabe, S. Iwata, K. Hashimoto, F. Misaizu, K. Fuke, J. Am. Chem. Soc. **117**, 755 (1995).
17. E.D. Glendening, D. Feller, J. Phys. Chem. **99**, 3060 (1995).
18. P.B. Armentrout, Acc. Chem. Res. **28**, 430 (1995).
19. C.T. Scurlock, S.H. Pullins, J.E. Reddic, M.A. Duncan, J. Chem. Phys. **104**, 4591 (1996).
20. C.S. Yeh, J.S. Pilgrim, K.F. Willey, D.L. Robbins, M.A. Duncan, Int. Rev. in Phys. Chem. **13**, 231 (1994).
21. M.H. Shen, J.M. Farrar, J. Chem. Phys. **94**, 3322 (1991).
22. F. Misaizu, M. Sanekata, K. Fuke, J. Chem. Phys. **100**, 1161 (1994).
23. M. Sanekata, F. Misaizu, K. Fuke, J. Chem. Phys. **104**, 9768 (1996).
24. S.G. Donnelly, J.M. Farrar, J. Chem. Phys. **98**, 5450 (1993).
25. D. Lessen, R.L. Asher, P.J. Brucat, J. Chem. Phys. **95**, 1414 (1991).
26. R.L. Asher, D. Bellert, T. Buthelezi, G. Weerasekera, P.J. Brucat, Chem. Phys. Lett. **228**, 390 (1994).
27. R.L. Asher, D. Bellert, T. Buthelezi, P.J. Brucat, Chem. Phys. Lett. **227**, 632 (1994).
28. R. Bouyer, F. Roussel, P. Monchicourt, M. Perdrix, P. Pradel, J. Chem. Phys. **100**, 8912 (1994).
29. P. Pradel, L. Poisson, J.P. Visticot, J.M. Mestdagh, C. Rolando, J. Chem. Soc. **93**, 1697 (1996).
30. D.E. Clemmer, Y.-M. Chen, F.A. Khan, P.B. Armentrout, J. Phys. Chem. **98**, 6522 (1994).
31. C. Lee, H. Chen, G. Fitzgerald, J. Chem. Phys. **102**, 1266 (1995).
32. N.F. Dalleska, K. Honma, P.B. Armentrout, J. Am. Chem. Soc. **115**, 12125 (1993).
33. C.L. Haynes, Y.-M. Chen, P.B. Armentrout, J. Phys. Chem. **100**, 111 (1996).
34. J. Berkowitz, G.B. Ellison, D. Gutman, J. Phys. Chem. **98**, 2744 (1994).
35. K.P. Huber, G. Herzberg, *Molecular Spectra and Molecular Structure. IV. Constants of Diatomic Molecules* (van Nostrand, New York, 1979).
36. C.E Moore, *Atomic Energy Levels*, Circ. 467, Vol. II (NBS, US Dept. of Commerce, 1952).